Experimental Investigation into a Novel Modular PEMFC Fuel Cell Stack.

P. Scott[1]*, R. Calay[2], Y. Chen[1], F. Bhinder[3].

[1]University of Hertfordshire, Sustainable Energy Technology Centre, Hatfield, Herts, AL10 9AB, UK.

[2]HiN, Lodve Langes Gate 2, PO BOX 385 N-8505, Narvik, Norway.

[3] Euro Energy Solutions Ltd, Enfield, Middlesex, EN3 6UE

[*] corresponding author, p.e.scott23@gmail.com

Abstract

The Polymer Electrolyte Membrane Fuel Cell (PEMFC), despite being regarded as an ideal replacement to the internal combustion engine, is still not an economically attractive prime-mover due to a number of key challenges that have yet to be fully resolved; such as degradation to cell components resulting in inadequate lifetimes, specialised manufacturing processes and poor gravimetric/volumetric energy densities. This paper presents a stack concept which removes the conventional bi polar plate (BPP), a component that is responsible for a large proportion of stack cost and volume in traditional fuel cell stack designs. The stack architecture compromises of active and passive components which are suited to mass manufacture and maintain functionality that the BPP fulfilled. Furthermore, the design allows the implementation of a fault tolerant system which can bypass faulty cells while still ensuring electrical output. The stack architecture is presented and characterised over a number of operating scenarios. The experimental studies suggest that the performance of the new design is similar to that of traditional stacks over a number of operating conditions despite the removal of the BPP and the FTS continued to operate at a desired operating criterion despite the loss of a cell within the stack.

Keywords: Hydrogen, PEMFC, BPP, MPP, Stack, Experimental, Electrochemistry.

1 Introduction

It is widely regarded that the PEMFC is one of the most promising solutions for clean and sustainable power production for future generations that will reduce our dependency on fossil fuels. The PEMFC is particularly attractive due to its simplistic operating principle, low operating temperature and its versatility to meet a wide range of applications over a large power demand spectrum without the need for much modification to either stack or overall system design [1,2]. Despite the considerable research and many feasibility studies undertaken on the PEMFC over various applications, the PEMFC is only just reaching a stage where it can be classed as commercially available, yet still not economically viable; a situation the fuel cell must be in before it can be considered as a suitable alternative to traditional prime-movers such as the internal combustion engine. Despite the simplistic operation which has made the PEMFC so favourable as an alternative prime-mover, it is fraught with a number of inter-related technological and operational issues which have led to the slow development of the PEMFC which must be resolved before widespread commercialisation is realistic [3]. Technological issues include material selection and subsequent manufacture of components while operational issues include optimisation of influential operating parameters and also prevention and management of component degradation within the fuel cell which directly relates to the durability and operational lifetime of the stack. However, the issues of cost and durability are also closely related, as often a reduction or a change in material selection to reduce the cost of the component will have a subsequent effect on the durability or performance of that component in the PEMFC environment. An example of this is a reduction of the Pt content on the catalyst layer to reduce cost, however at a loss of performance to a stack that has a higher Pt loading, or use of thinner perfluorinated, partially fluorinated or non fluorinated membranes which may be more susceptible to degradation mechanisms [4]. In order to meet the US DOE cost and lifetime targets set out for PEMFC components in the year 2015 which are based on automotive applications and 500,000 80KW stacks [5,6], it is

clear that a paradigm shift is required in stack design philosophy, material selection and fabrication techniques before these targets can be met.

One component in particular, the Bi Polar Plate (BPP), is responsible for over 30% of stack costs alone and contributes to over 60% of stack weight in some fuel cell designs and almost entirely all of the volume of the stack in the majority of stack designs [7]. The BPP is a multi functional component which is responsible for:

- Even oxidant and fuel distribution within the stack via an internal manifold design.
- Even gas distribution within each cell via a flow field design.
- Complete gas seperation between the fuel and the oxidant.
- Electrical conduction from one cell electrode to the adjacent electrode in the stack.
- Provide mechanical support to the stack.
- Facilitate thermal uniformity across the stack.

Furthermore, the hostile operating conditions inside the PEMFC means that the material must have excellent corrosion resistance, but also be highly electrically and thermally conductive while still be low cost, light weight and suitable for mass manufacturing processes.

At this stage, not a single BPP material meets all the requirements to perfectly satisfy the functionality and specifications of a BPP and subsequently there has been a trade off between material selection and the application of the plate [8]. The materials that have been of interest for BPP application can be broadly grouped into two categories, metallic based and carbon based. Traditionally, the BPP was made from graphite due to graphite's excellent corrosion resistance within the hostile acidic operating environment while exhibiting both electrically and thermally conductive properties, thus was deemed a suitable choice for the component. However, while graphite in theory is appropriate, its employment within a stack is not ideal from both a commercial and system viability stance for a number of applications where cost, system size, and system weight are important. The poor manufacturability of graphite results in high manufacturing costs [9] making graphite commercially unsuitable for large volumes of manufacturing. Furthermore, the porous and brittle nature of graphite means that in order to satisfy the criteria of the BPP, the BPP's must be made thick to improve both its gas impermeability and mechanical strength which increases the volume and weight of the stack, thus reducing the volumetric and gravimetric energy density of the stack. While traditional graphite BPP's that have been impregnated with a binding resin are on the decline, flexible graphite BPP's that expand natural graphite via an agent and heat treatment have been used more extensively, especially by Ballard Mark 900 series stacks[10]. While it does meet cost targets and has low contact resistance, it is mechanically weaker and has higher gas permeability than other BPP variants [10], therefore it cannot fulfil all criteria required for the ideal BPP.

Recently, considerable attention has been focused on the development of metallic BPP's and composite BPP's to reduce cost of manufacture while also producing a BPP that is suitable to the hostile acidic environment inside the PEMFC. Metallic BPP's offer, amongst other things, thinner section BPP's, high strength to weight ratios and orders of magnitude better electrical conductivity than carbon based BPP's, and can be manufactured economically in mass scale through stamping and hydro-forming techniques [10, 11]. It has been shown that metallic BPP's can be <0.5mm in thickness [10], therefore they are attractive for various applications where volumetric and gravimetric power densities are important. However, due to the hostile operating conditions, metals must have protective coatings to prevent passive oxidised layers forming on the surface of the BPP, which would increase electrical contact resistance and lead to metal ion dissolution and an increase in membrane resistance [10 - 12]. The coatings must have excellent electrical conductivity, strong adherence to the base metal which is being used as the BPP as to stop seperation from the metal and the coating and be corrosive resistance, while also meeting cost targets [8,10,12]. Many different coatings have been explored, ranging from gold, graphite's, nitrides and other inorganic coatings such as oxides and carbides [7, 8, 10]. The main issue with applying a metallic coating such as gold to a metal substrate is the mismatch in thermal expansion coefficient during thermal cycling [8, 10], which eventually causes delamination and exposes the base metal, often setting up localised galvanic cells which promotes corrosion at that area [10]. Applying a metal nitride such as titanium nitride has also been investigated, however these coatings can suffer from pinholing and cracks caused by uneven coating during the deposition process [8] making them susceptible to corrosion and metal ion leaching. A coating process can add complex techniques to the overall manufacturing stage, potentially offsetting the reduction in cost made through the material selection [12].

Composites do offer a solution in meeting both cost and performance targets as they can be manufactured using compression moulding and extrusion techniques which are commonly seen with plastics [10, 12]. These composites can be sub-divided into carbon-carbon composites and carbon polymer composites. Both sets of composites do offer qualities such as good chemical stability, good electrical conductivity and strength and the ability to mould the BPP into the desired shape using large volume manufacturing techniques [10], which is ideal from a cost point perspective. However, from a volumetric and gravimetric power density viewpoint, composites cannot compete with the extremely thin sections of metallic BPP's, with composites typically exceeding a cell pitch greater than 2mm, which is not suitable for certain markets [13].

Carbon-carbon composites are produced from carbon fibre / pheonilic resin slurry [8, 10] and then cured into shape. Chemical vapour infiltration thereafter promotes a carbon rich surface and makes the component impermeable to gases [10]. Issues occur with this type of BPP is that the manufacturing process is lengthy and can also suffer from a loss of dimensional tolerance of the BPP features [10] as the section cools in the mould. This can cause gas leakage and misalignment of plates after the stack has been assembled. Furthermore, the high operating temperature of the CVI step can result in the overall manufacturing process being expensive [10].

Carbon polymer composites allow injection/compression moulding techniques to be introduced, allowing rapid high volume outputs to be realised [8, 10, 14]. The composites are made from a thermoset or thermoplastic resin with an electrically conductive graphite filler such as natural graphite or synthetic graphite [8, 10, 15]. While these polymer composites have features of good chemical stability and lightweight, they often have lower electrical conductivities than other types of BPP material. This is due to a trade-off between mouldability and electrical conductivity to meet desired specifications. Lower ratios of graphite filler will make the BPP ideally placed for very high volume output. However, in order to reach suitable levels of electrical conductivity, graphite filler concentrations must be increased which results in less than ideal mechanical properties of the BPP, and the available manufacturing techniques are limited as a result of the high blend viscosity of the composite [14]. While graphite loading is typically between 60-80% [10, 16] it can be as high as 93%, thus it is clear that the amount of filler will have considerable effects on the attributes of the BPP such as overall porosity and density of the plate [10]. Carbon polymer composites also have issues with manufacturing processes. If injection moulding is used, then high graphite loading on the plate will reduce the flow of the melt through the screw, causing damages to the screw and mould, reducing the lifetime of the machinery [10]. Another issue associated with composite plates is the formation of a polymer skin around the BPP [17]. This polymer skin is a band of polymer rich, low electrical conductivity thermoset/thermoplastic which substantially increases the contact resistance between the BPP and the GDL [17]. Companies will have to use proprietary surface activation methods to remove this band and expose the inner layers of the BPP. These methods, such as abrasion or sanding, not only increase the overall manufacturing complexity and time of the part but it also leaves a rough surface exposed once the process has been completed [17]. This rough surface increases the contact resistance between the GDL and the BPP due to lack of an even surface for current collection, thus methods must be employed to further try and reduce this effect after the abrasion has taken place.

A small number of designs have been proposed which have either changed the stack architecture or utilised lightweight materials to improve the stack power density and/ or reduce the cost of the stack. Yi et al [9] designed a PEMFC stack where undulated Membrane Electrode Assemblies (MEA) were manufactured and combined with perforated metallic BPP's. The perforated plates were stamped into the undulate shape while the MEA's were hot pressed into the appropriate shape. Experimental analysis on a single cell indicated that performance improved as clamping pressure increased until catastrophic loss of output from MEA-BPP separation from clamping pressure. Based on the single cell, the volumetric power density was estimated to be 2,151.28 WL^{-1}, however, an experimental stack was not produced [9].

Murphy et al [18] designed a BPP that compromised of a series of metallic and polymer layers to create a gas tight seal between reactant gas flows while utilising metallic foamed plates for gas distribution. A gold coating was applied to the flow fields to minimise both the effects of degradation and electrical contact resistance. Murphy predicted that further design changes would result in a power density >1000WL^{-1}, however little mention was given to the cost of the BPP. A BPP which utilised a copper alloy corrugated BPP was designed and experimentally tested by Reddy [19]. The copper BPP's were produced using a wire ringer and pasted and supported using carbon tape and silver paint. Results indicated superior performance compared to

that of a traditional serpentine flow field BPP and that the use of the modified BPP reduced size by 11% and cost by 55% compared to that of the serpentine flow field BPP.

While considerable work has gone into the optimisation of the BPP in both material selection and design the component still contributes to a large proportion of weight and size to fuel cell stacks. Both metals and composites can offer the solution to material selection, cost, manufacture and performance however at this stage not one BPP can fulfil all demands.

Another problem that arises when utilising a BPP based stack architecture, aside from material and manufacturing limitations of the BPP, is that all cells within the stack are connected in series. As the number of cells in the stack increase, the risk of entire stack failure as a result of a cell failure rise accordingly. In larger stacks, for automotive applications for example, the number of cells included in a stack can be in the order of the hundreds, resulting in a higher risk of stack failure and also lengthy maintenance and repair times. If a single cell is malfunctioning then this can cause significant variations in cell voltages and uneven/unexpected heating in the region which will limit the fuel cell output or even severely damage components as a result [20]. The heating could also dry out membranes increasing the resistance of the membranes even further until rupture is possible. Often, cell voltage monitoring units (CVM) are added to fuel cell stacks to allow the operator to monitor each individual cell in the stack so that faulty cells can be quickly identified without significant damage to the surrounding components; however, this is merely a diagnostic tool and will not prevent loss of functionality.

Instead, the use of a mono-polar plate stack architecture can mitigate the risk of cell failure by allowing a fault tolerant system to be set up which allows faulty and ruptured cells to be bypassed while still ensuring operation of the fuel cell to continue. The stack will produce proportionally less power in relation to the number of cells that have been bypassed. Furthermore, less complex manufacturing processes are required to make mono-polar plate designs, as different materials suited to different manufacturing processes can be used to fulfil the functionality of the BPP [21]. Mono-polar plates can be utilised in two different configurations, laterally or in a pseudo- bipolar plate configuration [21]. The use of a lateral configuration has been mainly seen for low power, mobile applications where size and weight considerations are critical [21]. The lateral architecture can result in better volumetric packaging than BPP stacks, as the plates can be connected laterally as opposed to vertically, resulting in very thin, small and simple fuel cell stacks. This is especially true when the fuel cell stack is combined with a passive oxidant gas stream which removes a significant proportion of the Balance of Plant (BoP) required for fuel cell stacks [22]. For larger output/stacks, a pseudo bi-polar plate set up can be used which utilises MPP's [21]. Each pseudo BPP unit consists of two cells, with two cathodes on either edge, two anodes inside and a central fuel chamber which is shared between the two anodes [21]. The anode and cathode must be connected internally within each unit but then connected externally to the next unit making up the stack. Oxidant can be supplied either from free/ forced convection [21] from the atmosphere or through a manifold, as in a typically BPP configuration.

There is little published work on the implementation of fault tolerant systems within fuel cell stacks. Palma [20] investigated the performance of a 150W fault tolerant fuel cell stack by breaking a traditional series stack into a number of smaller sections each with its own isolated dedicated dc-dc converter. Each converter controlled 8 cells within the stack and each dc –dc converter was controlled by three push-pull modules. Each dc-dc converter was then electrically connected in series to the next section to produce a fault tolerant system. The proposed system had typical advantages such as [20] a) Power generation in each dc/ dc converter could be independently controlled; b) Extra heating in underperforming sections could be limited by reducing the load current on that section; c) Sections can be disengaged and bypassed if faulty.

Each module was programmed to have a total output voltage of 22V and up to 50W, as the concept was to produce a fault tolerant system, a single module should be able to provide the required maximum voltage of the system. However, during full load the fuel cell was rated at 12V. If a module voltage dropped below 3.8V during full load then that module would be disconnected. A control system was produced to control each section so that if a faulty module was identified the load could be reduced while a "healthy" module could increase the load current onto it to make up the deficit resulting in minimal power lost. This allowed cells that were performing satisfactorily to increase to their maximum current load capacity as opposed to being limited by the faulty cells. It should be noted that this could not be a long term solution due to the high temperature and mass

transport limitations often seen when running fuel cells at higher current densities. Testing of the stack showed that both normal and modular operation was capable with the second module bypassed and the stack producing electrical power of 87W. Furthermore, the authors stated that the stack could produce 10% more power than in a typical series configuration when using modular dc-dc converter system [20].

Alternatively, if a mono-polar system was used, then MPP's would connect external to the stack via electrical tabs or through a bus plate. A CVM would detect the individual voltages of the cells within a stack and then cells which are not operating could be bypassed by removing the connections from the bus plate.

A patent by Mclean [23] describes a fuel cell system where groups of fuel cells are electrically connected in series, and then connected to another group of stacks which are in parallel. The system is made up of many small fuel cells which have an active area between 1-5% of the total active area required in the fuel cell system. Mclean claims that the system provides passive fault tolerance for both open and closed circuit failures or for individual fuel cells. The system comprises of clusters of cells that are linked internally in series but are then connected to other clusters in parallel, thus allowing clusters to become redundant if required via the use of a diode placed in-between each cluster. As the active area of each cell is very small, and in the range of only 1-5% of total active area, a loss of a cluster would not significantly affect the total output of the system despite the cluster is redundant [23]. While the patent does provide fault tolerance, the system does require a significant number of small fuel cells, which makes the assembly and operation of the system complex. Each cell would have to be electrically connected to the other cell within the cluster, then each cluster electrically connected in parallel to another small cluster. As system size increases, the complexity of the reactant gas manifold design would also increase in order to ensure that each cell receives an even concentration of reactant gas. This patent does not discuss the size and weight penalties as a result of adopting this type of fault tolerance strategy.

Another patent, submitted by Fuglevand et al [24] describes a fuel cell stack system that utilises a number of PEMFC cartridges that each house 4 cells. These cartridges are monitored by a control system that can actively change the operating conditions of the input variables to ensure that the cells remain in an ideal state to produce power. The cells are all linked together via electrical contacts that are in series and are connected through a sub rack. The sub rack is then connected to a power bus in series via make before break electrical contacts. Thus, if any number of cartridges are taken out to be replaced or maintained the power output would reduce proportionally but the series connections would not be broken because these make before break connections. A CVM is applied to each cartridge to monitor the voltage of each cell within the cartridge which then sounds an alarm if the cartridge does not produce voltage that is expected, suggesting one or more mal functioning cells within the cartridge. Not only can cartridges be removed but also individual cells in the cartridges can be isolated and shunted as to not render full cartridges non-operational [24]. The approach does seem to provide a fully fault tolerant system, however the system does seem extremely complex when coupled with the full BOP and the use of cartridges, while offering flexibility in the power output and providing a fault tolerant system will add volume to the fuel cell stack due to the extra housing required to hold the cartridges themselves. Little mention was given to actual real time testing of the system and the cost involved of such a system.

It can be seen that there are a number of limitations associated with different types of BPP material and its use within a stack, and that not one material at this stage can fulfil all the functionality required from a BPP. Metals can achieve excellent volumetric and gravimetric power densities and electrical conductivity, yet can suffer from issues surrounding the stamping process of complex flow field patterns and the coating process required to prevent corrosion of the metal. Composites do offer a viable mass manufacture solution as they can be injection or compression moulded and are more chemically stable than metal BPP's. However, issues arise with lack of electrical conductivity, excessive wear to manufacturing equipment and the formation of insulative layers on the composite surface. At a stack level, the use of BPP's allows a simple series connection and a simple electron pathway from one cell to the next in the stack. However, this also makes the stack susceptible to failure if one cell becomes faulty or redundant. This paper tries to address these issues on two fronts. One is the design of an alternative stack architecture that splits the functionality of the BPP up into components and materials that are suited to the functionality and also can be manufactured using current large scale manufacturing processes without the need for unique IP processes typically seen with BPP manufacture. This aims to bring down the cost of the fuel cell stack by using materials that can be obtained readily. The second

area of this paper introduces the fault tolerance potential of the stack by utilising the stack architecture and bypassing a faulty cell yet still retaining a continuous electrical output from the stack.

2 Stack Design Concept

The design concept involves a series of identical chambers that provides a singular gaseous stock to two cells simultaneously with the fuel and oxidant alternating in each chamber. While only a single gas is fed into each repeated chamber, planar repeating cells are achieved by simply shifting cell boundaries to the middle of each chamber thus ensuring fuel and oxidant on either side of each MEA sandwiched between the repeating chambers.

Figure 1 presents the schematic of the stack architecture. Instead of a typical Anode –Membrane – Cathode/ Anode –Membrane- Cathode repeating configuration between the MEA of one cell through the BPP to the next cell in a traditional planar fuel cell, the following configuration is utilised; Anode- Membrane – Cathode / Cathode- Membrane – Anode/ Anode – Membrane- Cathode; whereby electrical continuity is achieved using perforated current collecting plates that allow for external connections in a series arrangement (and parallel if required) while also allowing a fault tolerant system to be implemented. This also means that the same initial sizing parameters, specifications and equations can still be used as with a traditional planar stack. The stack can be split into active and passive components. Active components are within the active area of the MEA and are present within the highly corrosive environment of the fuel cell. i.e. hot, humid and acidic conditions. The components include MPP's and a flow field plate. The MPP must be electrically conductive but also corrosive resistant, whereas the flow field plate must be chemically stable and provide structural rigidity to the stack. Passive components are designed to provide gas distribution of reactant gas streams to each cell in the stack and to provide structural rigidity and compression to the stack. These components need to be light weight, impermeable to gases, and rigid. The passive components are end plates, external manifolds and the cell housing.

External manifolds provide fuel and oxidant either side of the casing in a U arrangement. The stack has been designed with simplicity and manufacturability in mind and as such the main stack body compromises of just two components which have been mirrored on its inner planar face to create the overall stack components resulting in minimal need for change to the manufacturing processes. The novel design concept of the chamber means that the integrated chamber can be used for both gas streams by simply rotating the component by 180° thus ensuring the same repeatability that was achieved with the traditional BPP. The manifolds for both gas streams are symmetrical about the inner face of the manifold and are co-ordinated in relation to the chamber design. Within each chamber, an integrated insulating interdigitated flow topology is utilised to aid even gas distribution within the chamber and to the MEA's. The nature of the flow topology means that both diffusive and forced convection gas transfer mechanisms aid mass transfer to the reaction sites but also help to remove product water from the GDL and centralised flow field. Coated stainless steel (SS) BPP has been shown to meet material and cost targets set out by the US DOE and in particular can withstand the harsh acidic operating environment inside the PEMFC without significant oxide formation and metal ion dissolution, both of which are detrimental to fuel cell lifetime and performance [2, 25].

Titanium nitride (TiN) has been shown to reduce metal ion dissolution and contact resistance compared with that of uncoated SS while reducing the voltage decay as a result of corrosion to that of almost graphite [2]. Furthermore, TiN application is well established and is a relatively inexpensive process using vapour deposition. Here, perforated stainless steel plates with a TiN coating are used as the current collecting plates for each fuel cell which are housed within the repeating chamber. Perforations allow the gas to flow from the gaseous chamber to the GDL of each MEA sandwiched on either side of the chamber. The high density of the SS is offset by the perforations and the considerably thinner sheets to that of the graphite, despite SS having a density ~x4 to that of graphite. The simplified nature of the stack has meant that the compressive end plates are identical whether at the front or rear of the stack further reducing the machining processes required to produce the fuel cell stack.

The compressive end plates and the external manifolds' novel design form a gas tight seal between the two end plates and the stack chambers, ensuring no gas mixing or venting to the atmosphere can take place. While the number of components in the stack has increased, the manufacturing processes have been simplified. Perforated metal plates undergo a simple punching procedure and do not have the same dimensional tolerance constraints as that of a complex stamped BPP that may have intricate flow field and gasket designs.

Furthermore, the simple shape of the MPP can be easily formed by many cutting processes with minimal wastage. The casing can be made using standard injection or compression moulding techniques using thermoset/thermoplastics that are chemically stable. Not only does this ensure high volume output but also prevents excessive wear to the screw and mould which is typically seen with composite BPP's with high graphite filler content. The casing contains the MPP's inside it, which allows a cell pitch <2mm to still be realised, thus ensuring high volumetric and gravimetric power densities are achieved.

3 Fault Tolerant System

The fault tolerant system (FTS) allows the fuel cell to continue operating despite an MEA in the stack failing. The FTS can be achieved at both stack and system level dependant on the severity of the failure. At this stage, the implementation of the FTS at stack level is more relevant and therefore will be explained further. If a single MEA fails inside the stack then as expected the fuel cell stack will fail unless there is a change in the external connections which allows the fuel cell stack to bypass the failed cell. This is achieved by removing the external connections to the failed cell, connecting the cathode of the previous cell to the anode of the next cell, and restoring the electrical continuity of the stack. The power of the stack will reduce proportionally as a result of the lost cell with a reduction in the stack voltage as a result of a reduction of the number of cells in series. It will, however, allow the fuel cell to continue producing power despite the loss of a cell. Figure 2 is a schematic view that first illustrates the standard connections layout used in the stack architecture. Figure 3 illustrates the FTS principle when a cell has become faulty inside the stack.

With respect to the FTS shown in Figure 3, the fourth cell in the stack has ruptured and must therefore become redundant. The ruptured cell is shown as the patterned region, which contains anode 4 (A4) and cathode 4 (C4). The external interconnects from the cathode 5 (C5) are removed from the anode 4 (A4), while the connections between cathode 4 (C4) and anode 3 (A3) are also removed. Instead, cathode 5 (C5) is directly connected to anode 3 (A3) resulting in series connection within the stack. The remaining connections are not altered. The interconnects have been designed so that they can still be used in a FT mode despite the extra distance required to bypass a faulty cell. At this proof of concept stage, adjusting the external connections will be done manually, however, as part of a continued design process this process will next be achieved by an automated control process.

4 Experimental Apparatus and Procedures

As shown in Figures 4-5, a six cell 240 W (Pelec@nominal) modular PEM fuel cell stack was manufactured, assembled and characterised. The stack utilises 6 x 100cm^2 Active Area Nafion®117 five layer MEA with a Pt loading of 0.4mgcm^{-2} on carbon black with carbon paper used as the gas diffusion layer, sourced from Electrochem Inc. For the prototype fuel cell stack, acrylic (Perspex) was chosen as the material for chambers, external manifolds and internal flow field sections. Repeating chambers and external manifolds were manufactured out of house by Penta Precision Engineering® using CNC milling machines. The designs of the chambers and manifolds were such that they would be ideal to mass manufacture injection moulding techniques if large scale production was desired. Interdigitated internal flow field sections were manufactured in house using a CNC milling machine, where the interdigitated design was mirrored about the planar face, resulting in the same flow field design on both faces of the acrylic section. The flow field section was the same size as the active region of the chamber, and was coupled via an interference fit. SS 316 was used as the current collecting plates for both anode and cathode which was purchased in 0.5 mm thick pre fabricated perforated sheets which were then made to size using a laser cutter. The sheets were then coated with a ~2μm TiN layer via electron beam evaporation physical vapour deposition process by TecVac® coating services. Compressive gaskets were positioned between compressive end plates and external manifolds and between each repeating chamber. The gaskets varied in design however were both made from PTFE, with thickness 160μm +/-10μm. For initial proof of concept, the end plates were made from SS304; however, it should be noted that future stack designs will incorporate light weight compressive end plates as a part of a continual design improvement process. The stack was clamped via 8 x 8mm SS bolts through the central chamber casing and 8x 6mm SS bolts through the external manifold casing. Fluid connections were made via 12mm OD push fit connections.

External connections were made via the current collecting plates which protruded out of the repeating casings. The interconnects allow either a series, parallel, or both configuration within the fuel cell stack allowing complete flexibility depending on the power requirements of the application. During the prototype phase, interconnects were made from heavy duty insulated copper cabling with a unique electrical coupling to the current collecting plates to reduce interfacial resistances. During the characterisation phase, the connections were made in a series configuration, as shown in Figure 2. In order to evaluate the performance the fuel cell stack was assembled and characterised in house.

A CompuCell gas management system (GMS), purchased from Electrochem Inc, was employed to control, humidify and monitor both the fuel and oxidant gas streams. A TDI® Dynaload RBL800W was used for the load demand on the fuel cell stack of which power, current, voltage could be tested in a constant mode. The proprietary PowerStation® software was used to control gas flow, humidification, electronic load and data capture of all experimental variables during the testing phase. The GMS had three sub sections which controlled the flow of an oxidant (air), fuel (99.99% hydrogen) and an inert gas (nitrogen). The GMS utilised two MKS® Type 1179A mass flow meter/ controller (MFC) for all gas flows, whereby the purge flow flowed in both oxidant and fuel gas streams when in operation. The MFC had a Full Scale (F.S) volumetric flow of 25000sccm standard cubic centimetres for all gas flows, with a controllable range of 2-100% of the F.S. Uncertainty of the reading was 1% of the F.S, equating to 2500sccm, thus as the volumetric flow increases the precision of the flow reading improved. The GMS used a bubble humidification system for both the fuel and oxidant gas streams and was controlled through a proportional integral derivative control loop which heated de-ionised water to a temperature inputted by the user via ohmic heaters and was measured using type K thermocouples. Maximum operational water temperature was 110°C. The TDI RBL Dynaload is a resistive load bank which dissipated the received electrical load from the fuel cell in the form of heat. The Dynaload could be operated in four settings; constant current, constant power, constant resistance and constant voltage, of which all settings have three ranges dependant on the operational load of the fuel cell stack, with differing levels of precision of the measured response. Details of the available ranges and precision of the RBL Dynaload are presented in Table 1. The Dynaload had a programmable minimum operational voltage, which was chosen to be 0.2V per cell, resulting in an experimental shut down if the fuel cell stack voltage dropped below 1.2V. A stand alone Agilent® bench-top digital multimeter (34972a) was coupled with a 20 channel Agilent multiplexer unit (34901a) and was assembled, configured and commissioned for use as a cell voltage monitoring unit to measure the voltage distribution within the stack. Datalogger 3 was used for cell voltage data acquisition. Twin core insulated 20 AWG copper wire was used for all channels to minimise the risk of electrical shorting and disturbance from Electromagnetic and Radio frequencies. A schematic of the experimental rig is given in Figure 6 with associated sensor ID and position given in Table 2.

5 Results and Discussion

The stack was tested under various operating conditions and both dynamic and steady state load sequences. Details of the static inputs, variable inputs, test outputs and the measurement uncertainties of both the measureable inputs and outputs are given in Tables 3-7 respectively. Here, the performance of the fuel cell stack are presented over varying temperatures, oxidant stoichiometric ratios and steady state testing. Each test was repeated three times and the average results of the three tests are presented in Figures 7-12. Experiments were repeated over a period of three days for each test condition and are repeatable.

5.1 Effect of Operating Temperature on Stack Performance

The stack was subject to increasing operating temperature ranging from 303-363K with 20K increments while other global operating conditions were held under the following conditions: H_2/air @100% relative humidity, P_{stack} abs. 1.2 Bar (H_2/air), stoichiometric ratios (λ) H_2 2; air 3, while the current loading on the fuel cell stack was stepped up from 0-1.2 Acm^{-2}. The stack output over the range of temperatures is presented in Figure 7.

From Figure 7 shows that despite the considerable rise in the operating temperature of the fuel cell stack only a marginal improvement in the output of the fuel cell stack was achieved. This was attributed to a number of key issues that were identified during experimental testing. Low OCV's were recorded on throughout the testing phase on cell 5, with the voltage decreasing as the temperature increased. Of interest was that in

combination to the low voltage of cell 5, both end cells within the stack (cell 1 and cell 6) had marginally lower outputs compared with that of the central cells (cells 2-4) suggesting bulk transport limitations to the front and rear cells within the stack. As temperature increased, the output of cells 1-4, 6 followed a net trend that output increased as temperature increased, which is expected due to an improvement to the reaction kinetics of both the Hydrogen Oxidation Reaction (HOR) and the Oxygen Reduction Reaction (ORR) and an improvement to the convective and diffusive properties of the reactant gases. However, the output of cell 5 decreased as temperature increased which was identified to be as a result of reduction of oxidant to the chamber that supplies cells 5 and 6, as a result of excessive liquid water formation at the chamber inlet interface with the external manifold. This led to moderate drying out of the membrane due to rise in operating temperature of the fuel cell stack and the reduction of concentration of oxidant species at the catalyst layer which caused significant drop in cell output as the current loading increased. Thus only a marginal increase in stack output was seen as current density increased, with a maximum power density of 2.52Wcm^{-2} (0.42Wcm^{-2} per cell) seen at an operating temperature of 303K, however the improvement due to the rise in operating temperature was best seen at <0.2Acm^{-2} where a maximum stack OCV of 5.37V was recorded at 363K.

5.2 Effect of Oxidant Stoichiometric Ratio on Stack Performance

The stoichiometric ratio (λ) is the amount of reactant gas required to meet the current load with a fuel utilisation of 100%. In a theoretically ideal situation, 100% utilisation at all current demand would be achievable, however due to bulk and diffusive transport limitations, gas leakage and water management within the fuel cell stack, stoichiometric ratio of 1 would often result in poor performance and high concentration losses in some stack designs. Thus, typically this amount is multiplied by a factor to improve reactant gas concentration at reaction sites. Furthermore, normally air is used as an oxidant which brings a performance penalty as the concentration of Oxygen in air is ~0.21, thus increasing stoichiometric ratio of air is often essential to increase the concentration of Oxygen at the cathode catalyst layer. However, despite the decrease in fuel utilisation, higher λ will also help to improve the removal of product water at the cathode by increased evaporative action resulting from the higher flow rate of the oxidant. Here, the performance of the novel fuel cell stack is presented where the stoichiometric ratio of the oxidant was varied between λ=1-3 under the following global operating conditions: H_2λ=2; air λ=x; H_2/air @100% RH; P_{stack} abs. 1.2 Bar (H_2/air) Tcell=343K and is presented in Figure 8.

The effect of stoichiometric ratio on the output of the stack can be clearly seen at higher current densities. In Figure 8, the difference between the OCV's of the stack at different stoichiometric ratios were marginal, all recording an OCV > 5V, however as current density increased the difference in stack output as a result of the difference in λ was clear. The stack operating at λ=1 had a consistently lower output compared with that of λ=2;λ=3, and in fact output of stack was a clear trend where output=λ3>output=λ2>output=λ1 as expected. Operation of the stack at λ=1 resulted in a system shut down of the experimental testing at 0.80Acm^{-2} as a result of significant concentration losses occurring at cell 2, where concentration voltage drop occurred at 0.5Acm^{-2} through to 0.8Acm^{-2} and resulted in V_{cell2} dropping below 0.2V safety threshold. An increase in oxidant stoichiometric ratio to λ=2 resulted in an a subsequent improvement in stack output at all current loadings, indicating that doubling the stoichiometric ratio does increase the bulk and diffusive transport of oxidant to the reactant sites as expected despite the change in stack architecture. The increase in stoichiometric ratio also improved the limiting current density of the stack to 1.0Acm^{-2} with more uniform output from all cells within the stack; however cell 5 had a smaller output than other cells in stack. An increase in stoichiometric ratio to λ=3 saw an improvement in stack output again between current loading of 0.3-1.0Acm^{-2}. It can be seen that there was no improvement in the limiting current density of the stack; however this was a result of cell 5 significant drop in cell voltage resulting in experimental test shut down. Analysis indicated that similar to what was seen during temperature dependency; liquid water accumulation at the inlet to the oxidant chamber of cell 5 and 6 resulted in reduced bulk gas flow to that cell and concentration loss at higher current densities despite an improvement to limiting current density for other cells in stack. Operational benefits of operating at higher stoichiometric ratios were clearly visible through stack power output. The maximum power output achieved at λ=1 was 178.4W @ 0.6Acm^{-2}, whereas maximum power achieved at λ=2 was 202.7W @ 0.7Acm^{-2} and λ=3 was 225.9W @ 0.8Acm^{-2} respectively, a 47.5W increase in stack power as a result of improving the stack voltage at higher current densities.

As a result of the variation in stoichiometric ratios and operating temperature the maximum output recorded by the fuel cell stack was identified, as shown in Figure 9. Operating conditions of the fuel cell stack were as follows: T_{cell}=348K; H_2/air @100% RH; P_{stack}(abs) 1.2Bar(H_2/air); stoichiometric ratios: $H_2\lambda 2$;air$\lambda 3$. Stack peak power was measured at 234.56W, with a power density of 0.390 Wcm^{-2} and a nominal electrical output (0.6Acm^{-2}) of 210W. As current density increased past 0.8Acm^{-2} (max. power output) the power output from the stack decreased considerably. This was primarily attributed to the repeated sudden drop in cell potential from cell 5 as a result of concentration losses as already seen under different test conditions, therefore operation of the stack at higher current densities results in less than ideal output, even under optimised conditions.

5.3 Steady State Testing

Steady state testing involves the fuel cell stack being maintained at a desired output for an extended period of time and monitoring the behaviour of the cells during the test sequence. Here, the fuel cell stack was subjected to a stack voltage of V_{stack}=3.6V for 1440 minutes with polarisation curves taken at 0mins, 720mins and 1440 mins under the following operating conditions T_{cell}=348K; H_2/air @100% RH; P_{stack}(abs) 1.2Bar(H_2/air); stoichiometric ratios: $H_2\lambda 2$;air$\lambda 3$. The cell voltages within the stack under V_{stack} =3.6V are presented in Figure 10 [excluding polarisation curve testing].

Whilst the fuel cell was kept at 3.6V, cells 5 and 6 were erratic during different stages in the testing process. After pol.1@t=0mins, cell 5 took 320 minutes to rise from an operational voltage of ~0.3V to that of the $P_{nominal}$ of ~0.6V required per cell. As seen in Figure 10, cells 1-4, 6 operated between 0.66-0.73V in order to compensate for the low voltage seen in cell 5. Of the cells to compensate, cell 2 was consistently at a higher operating voltage approximately operating at >0.7V for over 700 minutes. After 320mins, cell 5 begins to stabilise towards that of $P_{nominal}$, bringing the operating voltages of cells 1-4, 6 towards that of the desired 0.6V per cell. However, it can be seen that cell 5, despite a rise in operating voltage, remains consistently lower than the respective cells in the stack, with a 0.06V drop in operational voltage compared with that of cell 2. After 320 mins, the cells have a period of stabilisation where all cell voltages are within 0.1V tolerable range. After t=720mins it can be seen that cell 6 now is considerably unstable with regions of significant cell voltage drop close to the emergency shutdown voltage of 0.2V. The gradual drop in voltage followed by a sudden drop of voltage is characteristic result of flooding first within the GDL, seen by a gradual decrease in cell voltage followed by flow channel blockages resulting in a significant drop of reactant gas concentration leading to starvation to the cell. This is in agreement with the results found by Fouquet [27] where sudden voltage drops were also seen as a result of water blockages. As the pressure builds up inside the flow channels the water is then removed, eventually restoring the performance for a period of time. Cells 1-5 compensated the fluctuations in voltage of cell 6 which maintained the desired V_{stack} =3.6V, however as a result set up a quasi- dynamic phase where the cells were consistently varying in response to the changes to cell 6.

The cyclic voltages of cells 5 and 6 throughout all test sequences suggest that bulk reactant gas distribution is responsible for the varying performance in these cells. It can be seen that performance of the fuel cells are satisfactory if reactant gases reach the active areas of the membrane, which suggests that bulk distribution of reactant gases is suitable, if somewhat rich, towards the rear of the stack as seen by the consistent performance throughout of cells1-4. However, the unstable behaviour of cells 5 and 6 simultaneously during different test sequences indicated inherent issues with bulk oxidant distribution to the chamber at higher current densities and led to poor cell output characteristic of that caused by concentration losses. The concern lies in degradation [28] mechanisms acting on both the affected cells and the supporting cells as a result of the erratic performance of cells 5 and 6. Cells 5 and 6 are likely to suffer from gas starvation mechanisms that can result in Carbon and Pt particle oxidation, cell potential reversals and degradation as a result of repeated oxidation and reduction of the catalyst layers.

5.4 Fault Tolerant System

The stack was operating in a steady state setting of V_{stack}= 3.6V with the following global operating conditions used: H_2 λ=2; air λ=3; H_2/air at 100% RH; P_{stack} (abs) 1.2Bar (H_2/air); T_{cell}=80°C. The stack was set at V_{stack}=3.6V, and as seen in Figure 11 the cells are operating at V_{cell} ≥0.66V and maintaining this voltage. At

t=52 minutes (t=2minutes given above) cell 5 suffered a catastrophic loss of voltage where as a result the polarity of the cell was reversed. As a consequence of the catastrophic loss seen in cell 5 the emergency shut off was activated, stopping the test sequence. Once the current flowing through the stack had been removed the electrical connections to cell 5 were removed and the FTS implemented using the connections shown in Figure 3. One concern while changing the connections was that if there was no load imposed on the fuel cell stack while reactant gases were present inside the stack then that would bring the cells up to an OCV, where degradation can take place. The FTS implementation took <30 seconds, minimising the effects of operating at OCV. Upon restarting the test sequence the remaining cells in the stack maintained the V_{stack}=3.6V requirement, as shown by a shift up in voltage after the FTS implementation in Figure 11. As the condition was to maintain the stack voltage in this scenario, and there was one less cell in the stack that the voltage of each cell increased, however at a sacrifice to the current density which dropped proportionally to the voltage step up.

Figure 12 presents the variations in stack output as a result of the FTS implementation. With reference to Figure 11, all cells maintain a voltage of V_{cell} ≥0.74V in order to uphold the desired V_{stack}=3.6V. It is clear that cells 1-4 have a consistently higher output than that of cell 6, with a V_{diff}~0.07V between cell 2 and cell 6 consistent throughout the FTS implementation. Cells 1-4 have very uniform voltage outputs and have an operational voltage variance of 0.03V between the max-min cells within that group. It can also be seen that there are slight variations in output for all active cells as the time increases in order to maintain the desired stack output. While cell 6 is clearly producing less output than cells 1-4, it does seem to follow the same voltage variance as cells 1-4 suggesting that the cell is not suffering from significantly higher Ohmic losses than the other cells in the stack.

With respect to Figure 12, as a result of the voltage increase of cells 1-4, and 6 there was a drop in current which as a result also dropped the power output from the fuel cell stack. As the FTS is designed to continue power output even after a cell failure, there will naturally be a drop in power output proportional to the number of cells that have been made redundant. In this case, one cell has been removed, therefore during steady state operation this equates to a P_{elec} drop ≤50W. Furthermore, depending on the system requirements at the time, this P_{elec} may drop even further if a voltage is required to be maintained, as the current density will have to drop, resulting in a lower power output. In this case, there was a current density drop from 0.57A/cm^2 to 0.31Acm^{-2} in order to maintain the V_{stack}, thus reducing the P_{elec} further. The drop in the P_{elec} was significant, with P_{max}=197.9W before the implementation of FTS and dropping to a P_{min}=102.6W at the lowest current density. It can also be seen that the current density also fluctuates slightly as a result of the load change, which has a direct effect on the P_{elec} of the stack. Immediately after the change, the P_{elec} drops to ~115W, then drops further to ~108W and 102W momentarily before stabilising at P_{elec}~109W where it maintains this output.

The implementation of the FTS resulted in continued and stable stack output at the desired load setting despite the loss of a cell in the stack. The stack was tested under the FTS setting for a further 20 minutes with no significant issues seen. In order to maintain the desired voltage, the overall output reduced as a result of a reduction in current density. Further testing is required under different load settings to ensure stack behaviour remains stable under FTS.

5.5 Summary of Experimental Results

An alternative PEM fuel cell stack architecture which includes fault tolerance has been designed, assembled and experimentally characterised. Characterisation of the fuel cell stack indicated that the change in stack architecture led to both cell and stack performance that is suitable and similar to traditional designs under certain operating conditions. However, characterisation also indicated that there was issues with the mass transport into an oxidant chamber which supplied cells 5 and 6 simultaneously, resulting in lower than expected outputs and erratic behaviour. As operating temperature of the stack increased, cell 5 output decreased considerably, offsetting smaller gains made from other cells in the stack. As oxidant stoichiometric ratios increased cells 1-4, 6 increased significantly while the output of cell 5 reduced which limited the gains made in stack output. During steady state output, both cells 5 and 6 had periods of unstable behaviour. In order to maintain the desired stack voltage of 3.6V remaining cells in the stack varied to keep this desired voltage constant, however this resulted in quasi dynamic phases where all cells in the stack were varying with respect to the erratic output of cell 5 or 6, increasing the likelihood of degradation mechanisms taking place.

After the rupture of cell 5 in the stack, the FTS was implemented. A change in electrical connections was achieved < 30 seconds, minimising the negative effects of operating at OCV. The FTS was successful in maintaining the designed stack requirement of a steady voltage of 3.6V, now with 5 cells instead of 6. However, in doing so the stack power output dropped considerably. The loss of one cell from the stack dropped the output by less than 50W, but in order to maintain the stack voltage the current density of the cells reduced to increase the voltage output from each cell. In doing so, the stack output dropped even further, resulting in an overall electrical power drop of 95.3W, stabilising at a power output of 109W, originally being 197.5W. Despite the loss of a cell, the stack continued to operate under steady state conditions indicating the FTS did work and was a viable short term system that could allow continued power output despite cell failure.

5.6 Limitations of the Design

There are a number of limitations associated with this type of stack architecture. The use of MPP results in an external connection being made with copper wire over a larger distance that would be seen with a traditional BPP design. The connections between the MPP tab and the copper wire must be connected securely in order to minimise interfacial resistances between the connecting wire and the MPP. Good contact was achieved by bolting the two surfaces together. The voltage loss seen with this stack would be higher than that of a traditional stack design, as the electron pathway is longer and would travel through more material. In order to mitigate this issue, the overall stack output would need to be regulated and only a small operating band would be suitable for this design. Lower current density operation, and a higher voltage per cell would minimise contact resistance at the interconnects due to a reduction in overall current in stack. The stack design could suit smaller active area membranes, which would reduce the distance electrons, need to travel in the plane of the MPP to the tab to connect to the next cell, also reduce the current through the stack, but would increase the number of external connections that would need to be made. Current distribution through the current collectors has not been investigated, and is a topic for further work. This stack architecture also has limitations not only on current collection but also heat management. The stack casing being made from plastic does cause issues with effective heat management at larger electrical power outputs. The design currently utilises convective cooling through the oxidant gas stream, which is suitable for power outputs less than 1kW. For power outputs above 1kW, a cooling fluid such as water is typically needed to remove heat from the stack, and relies on good thermal conductivity of the material to transfer heat away from active area to the fluid. Here, the plastic casing does not have suitable thermal conductivity effectively locking in the temperature inside the cells. An engineering plastic that has good chemical stability, structural rigidity and thermal conductivity would be needed, which could increase the cost of the stack due to a rise in cost of the raw material. Despite the limitations, in certain applications, such as military, a fuel cell system which comes with fault tolerance built in is attractive, therefore there is a scope for this design to enter select markets.

Further work is focused on improving the reactant gas distribution to this oxidant chamber, further weight saving improvements and continued characterisation.

6 Conclusions

- An alternative fuel cell stack was designed, assembled and experimentally characterised.
- The fuel cell architecture has lead to the removal of the BPP and instead a series of chambers that supply a reactant gas to two cells simultaneously via an external manifold has been utilised.
- The design also incorporates a fault tolerant system which allows faulty cells to be bypassed and the fuel cell stack to continue. This feature is typically not available for traditional BPP stack's which are connected in series.
- All components inside the stack can be manufactured using mass manufacturing techniques and as such the stack design is a significant step towards moving away from complex manufacturing processes typically seen with graphite BPP's and other material variants. TiN coated SS316 stamped plates are utilised for current collection benefiting from higher electrical conductivity while being suited to mass manufacture stamping processes. Connections were made external to the stack, which not only increases versatility but also allows the implementation of a fault tolerant system.

- Stack characterisation suggests that stack performance is similar to traditional designs under certain operating conditions. There were issues with bulk oxidant transport into one of the oxidant chambers resulting in erratic cell output from cells 5 and 6. As temperature increased, the output of all the cells in the stack increased, however gains in output were marginal as a result of the poor cell output from cell 5 as temperature increased. The effect of oxidant stoichiometric ratio on the fuel cell stack saw considerable improvement in stack output from λ=1 increasing to λ=2, with improved performance as current density increased and an increase in limiting current density of the stack from $0.8Acm^{-2}$-$1.0Acm^{-2}$. Small gains were seen as λ=2 increased to λ=3, however this may have been limited by erratic output of cell 5 as the stoichiometric ratios increased, offsetting the gains made by improved output from the other cells in the stack.
- Steady state stack voltage was achieved; however voltage monitoring indicated that erratic behaviour from cells 5 and 6 resulted in quasi dynamic output from other cells in stack to maintain desired stack voltage. In particular, cell 2 responded to the changes in cells 5 and 6 more than other cells in the stack. The behaviour from cell 5 and 6 had the same characteristics as that seen by previous research by Fouquet, where erratic behaviour was assigned to cell flooding.
- The FTS system plays an important role in reliability of the new stack design. The FTS system maintained the cell stack voltage of 3.6V at a steady state despite the loss of functionality of cell 5 while the current density dropped to maintain the voltage criterion but continued to operate.
- Further work is focused on improved bulk oxidant gas distribution and more weight savings made to stack architecture.

Acknowledgements:

The authors would like to thank the EPSRC and Euro Energy Solutions for their financial contributions.

Nomenclature

i	Current density/ Acm^{-2}
P	Pressure, Power/ Bar, Watts
T	Temperature/ K
V	Voltage/ V
Greek symbols	
λ	Stoichiometric ratio
Subscripts	
Stack	Stack output
Cell	Cell
Nominal	Nominal operating point

References:

[1] M. Grujicic, K. Chittajallu, *Applied Surface Science* **2004**, *227*, 56-72.

[2] P. Hentall, J. Lakeman, G Mepsted, P. Adcock , J. Moore, *Journal of Power Sources* **1999**, *8*,

[3] N. De Las Heras, E. Roberts, R. Langdon, D. Hodgson, *Energy and Environmental science* **2009**, *2*,206-14.

[4] F. De Bruijn, V. Tam, G. Janssen, *Fuel Cells* **2008**, *08*, 3-22.

[5] J. Sinha, S. Lasher, Y. Yang, *TIAX LLC* **2010**.

[6] C. Johnston, Y. Kim, E. Brosha, *Los Alamos National Lab* **2010**.

[7] A. Hermann, T. Chadhuri, P. Spagnol, *International Journal of Hydrogen Energy* **2005**, *30*, 1297-1302.

[8] P. Hamilton, B. Pollet, *Fuel Cells* **2010**, *10*, 489-509

[9] P. Yi, L. Peng, X. Lai, D. Liu, J. Ni, *Fuel Cells* **2010**, *10*, 111-117.

[10] D Brett, N Brandon, Journal of fuel cell science and technology 2007, 4, 29-44.

[11] K. Feng, G. Wu, Z. Li, X. Cai, P. Chu, *International Journal of Hydrogen Energy* **2011**, *36*, 13032-13042.

[12] L. Nguyen, F. Mighri, Y. Deyrail, S. Elkoun, *Fuel Cells* **2010**, *10*, 938-948.

[13] A. Martin, L Joerisson, Autostack, -creating a European stack cluster, Fuel cell seminar and expo, 2011.

[14] F. Mighri, M. Huneault, M. Champagne, *Polymer Engineering and Science* **2004**, *44*, 1755.

[15] A. Muller, P. Kauranen, A. von Ganski, B. Hell, J. Power Sources 2006, 154, 467–471.

[16] H Kuan, C. Ma, M. Chen, S. Chen, J. Power sources 2004, 134, 7-17.

[17] B Avasarala, P. Haldar, J. Power Sources 2009, 188, 225-229.

[18 O. Muprhy, A. Cisar, E. Clarke, *Electrochemica Acta* **1998**, *43*, 3829-3840.

[19] V. Nikam, R. Reddy, *International journal of Hydrogen Energy* **2006**, *31*, 1863-1873.

[20] L Palma, P Enjeti, IEEE trans. Power electronics 2009, 24, 1437-1443.

[21] D Jiang, R Chu, J Power sources 2001, 93, 25-31.

[22] Y Chan, T Zhao, R Chen, C Xu, J Power Sources 2008, 178, 118-124.

[23] G Mclean, *US 2,009,028,039,0* US, 2009.

[24]W Fuglevand, S Bayyuk, G Lloyd, P Devries, D Lott, J Scartozzi, *6,773,839* US, 2004.

[25] J. Wind, R. Spah, W. Kaiser, G. Bohm, *Journal of Power Sources* **2002,** *105*, 256-60.

[26] TDI Power, *TDI Dynaload division RBL 488-800 operation and programming manual* **2004.**

[27] N. Fouquet, C. Doulet, C. Nouillant, G. Dauphin-Tanguy, B. Ould-Bouamama, *Journal of Power Sources* **2006**, *159*, 905-13.

[28] P. Scott, *Thesis*, University of Hertfordshire, UK, **2012**.

Figure Captions:

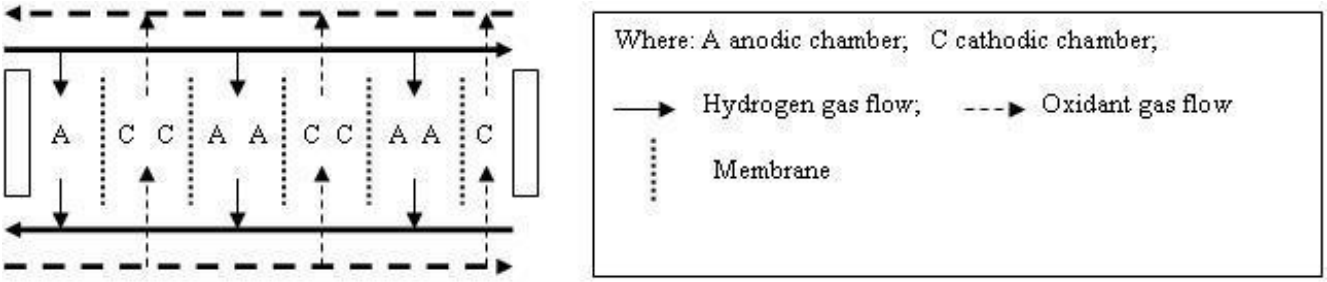

Figure 1: Schematic of novel stack architecture arrangement.

Figure 2: standard connections layout

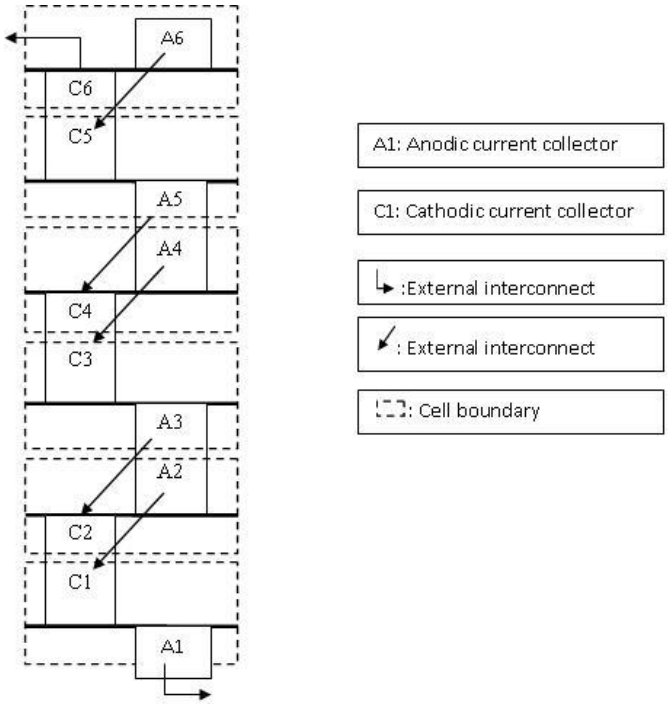

Figure 3: FTS layout

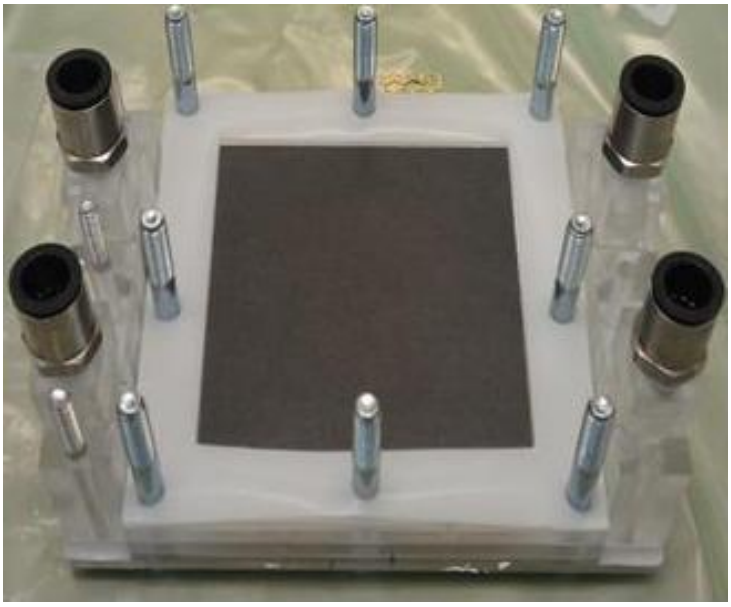

Figure 4: Assembly of PEM fuel cell stack.

Figure 5: Novel PEM fuel cell stack.

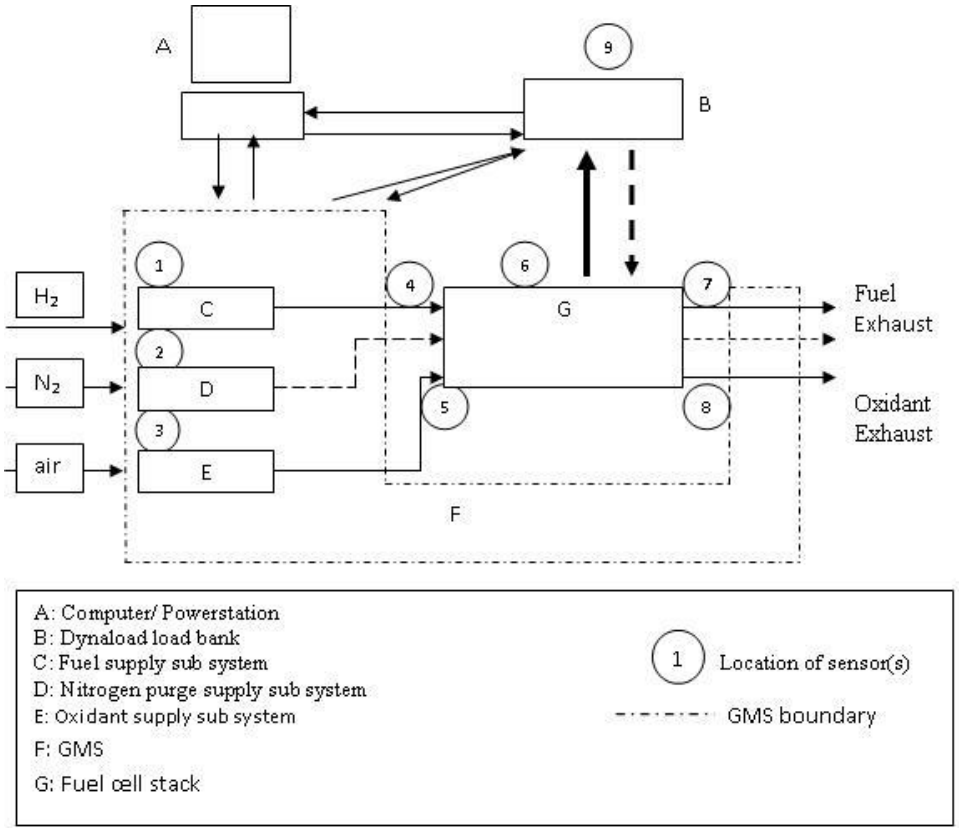

Figure 6: Schematic of experimental rig

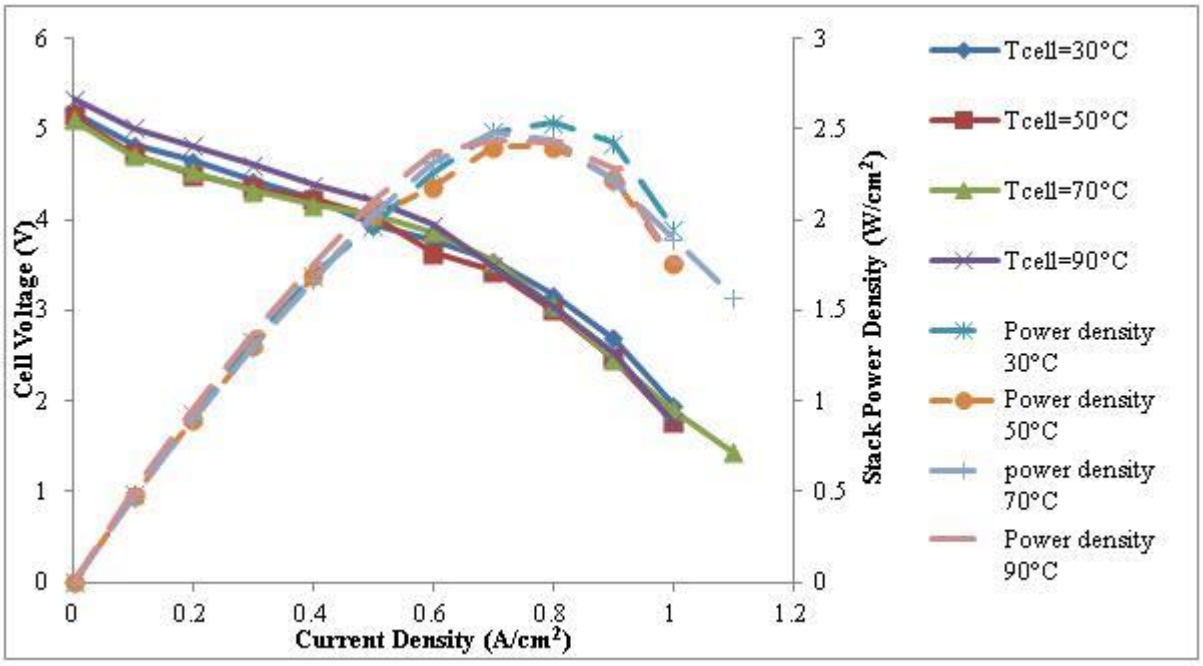

Figure 7: Stack output with respect to operating temperature.

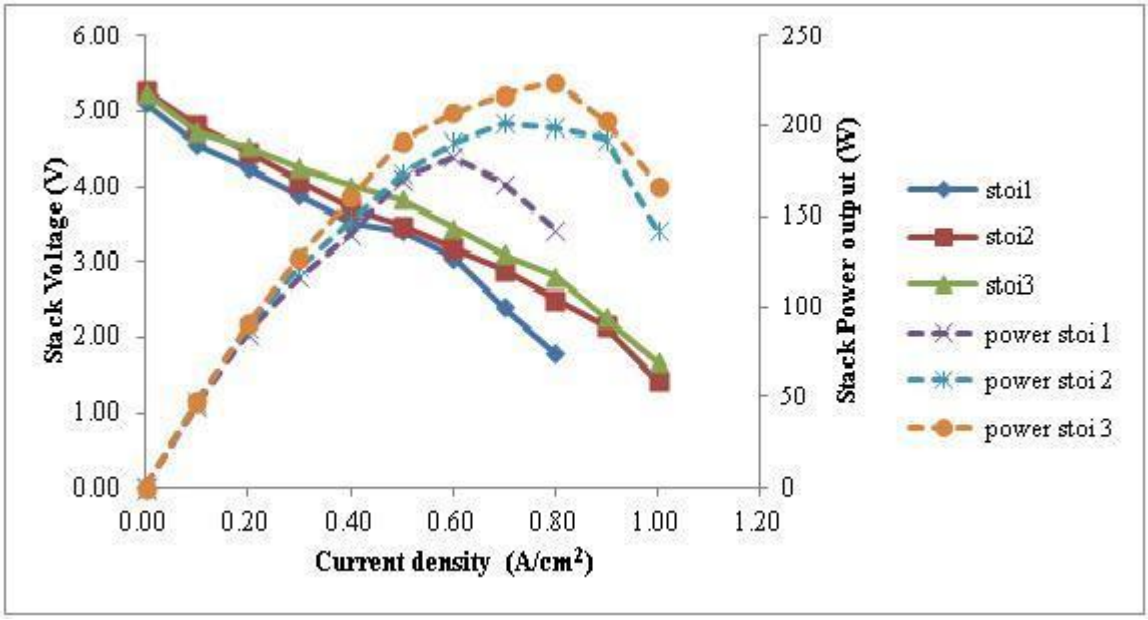

Figure 8: Stack output with respect to oxidant stoichiometric ratio.

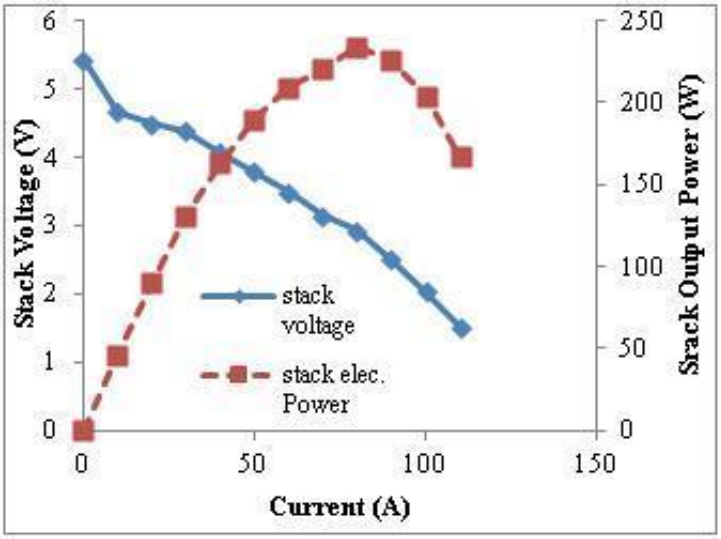

Figure 9: Maximum power output achieved from novel fuel cell stack.

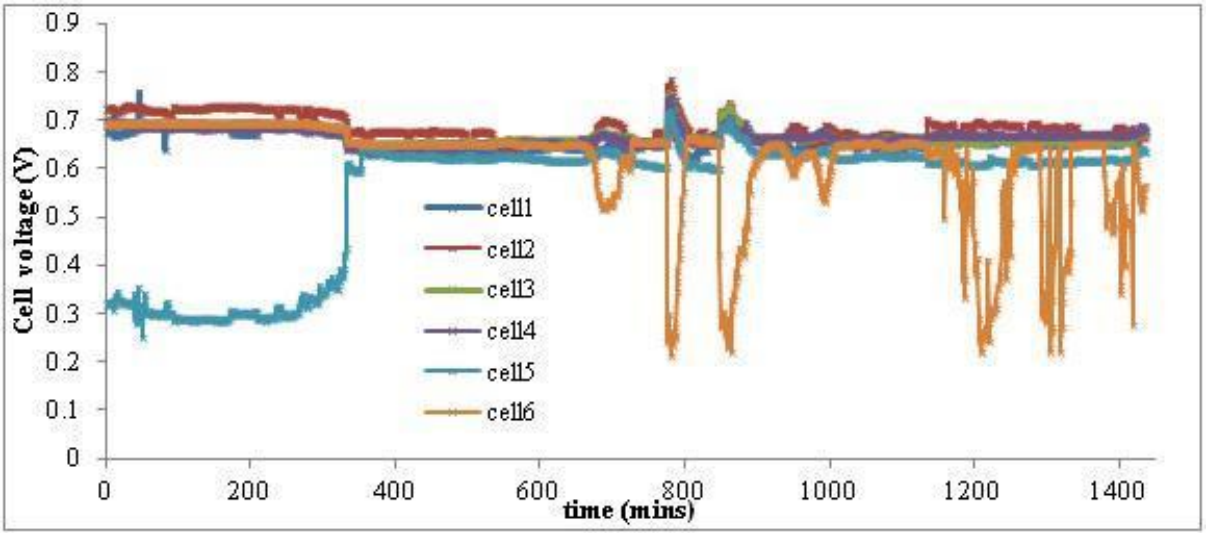

Figure 10: Voltage monitoring of cells 1-6 during steady state testing @Vstack=3.6V.

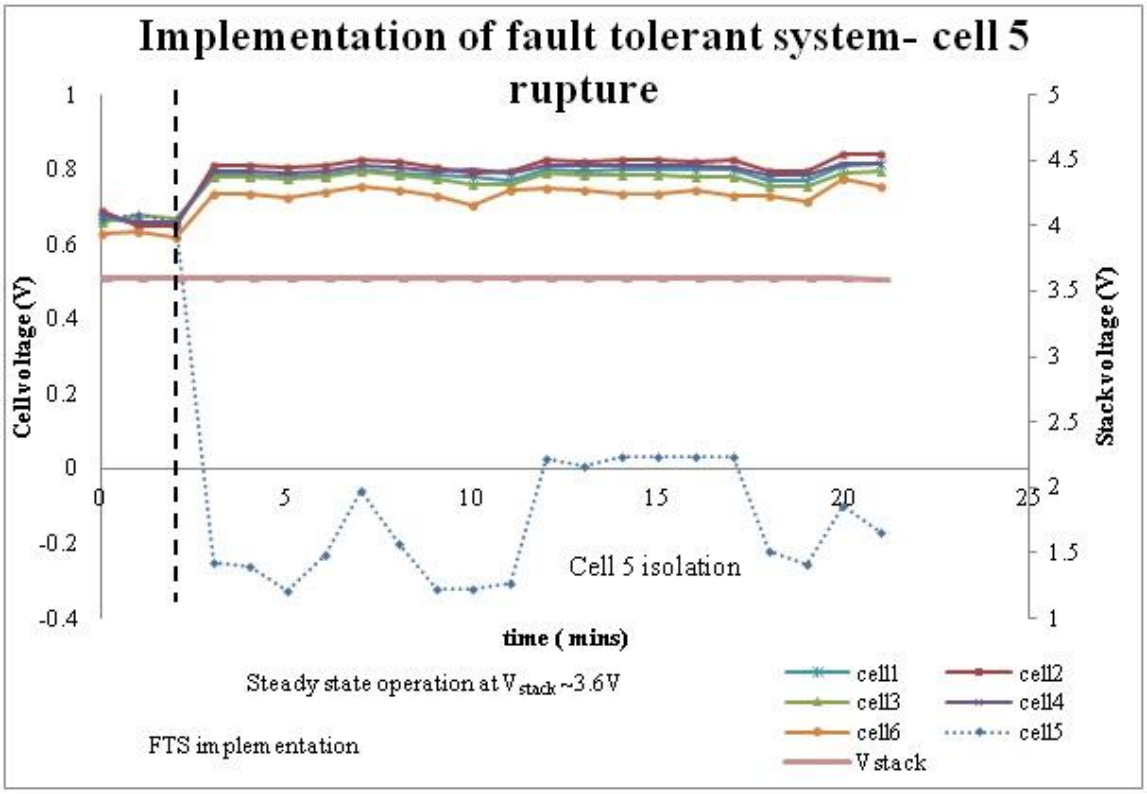

Figure 11: FTS implementation

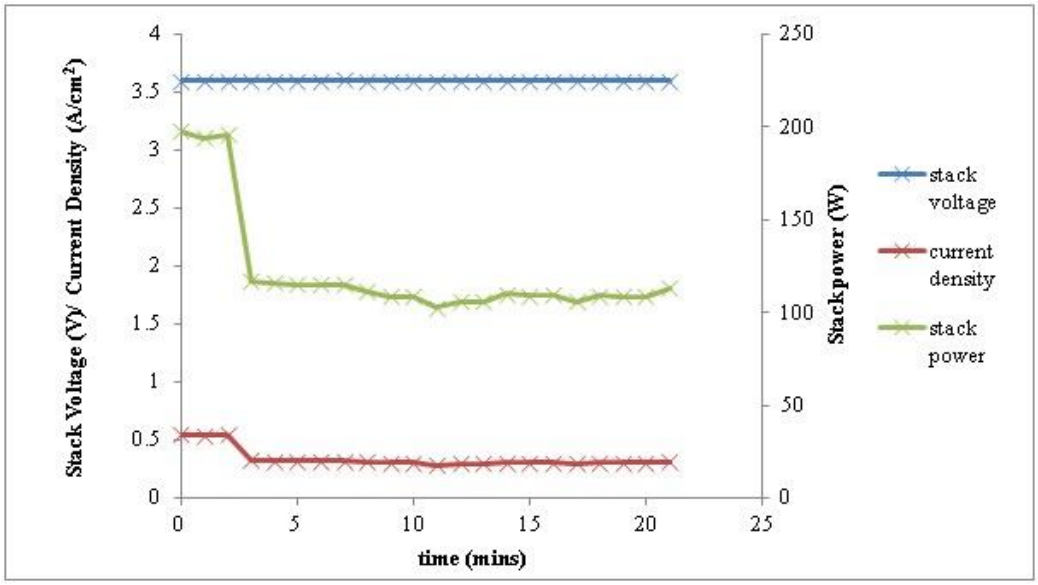

Figure 12: fts implementation on stack output

Tables:

Table 1: Dynaload operational settings and associated measurement uncertainty [26].

Type of load	**Range**	**Measurement uncertainty**	**Additional information**
Constant current density	Low: 2 Amps Med: 20 Amps High: 120 Amps	±0.5% F.S ±0.25% F.S ±0.25% F.S	Regulation: ±0.1% of F.S Resolution (IEEE): 1/4000 of F.S Load disconnect @105% F.S
Constant voltage	Low: 10 V Med: 50 V High: 100 V	±0.5% F.S ±0.25% F.S ±0.25% F.S	Regulation: ±0.15% of F.S Resolution (IEEE): 1/4000 of F.S Load disconnect @105% F.S
Constant power	Range: < 800W	±3% of F.S	Regulation: ±3% of F.S Resolution(IEEE):±0.25% of F.S

Table 2: Sensor ID and position during experimental testing.

Sensor description	**Sensor location**	**Sensor ID**	**Sensor type**	**Sample rate**
Stack current	9	I-0	Potentiostat	1/sec 1/5 sec^ 1/min
Stack voltage	6	V-0	Potentiostat	
Cell voltage	6	Vn –(Vn-1)	Voltage multiplexer	
Fuel gas inlet temperature	4	TF1	Thermocouple type K	
Fuel gas outlet temperature	7	TF2	Thermocouple type K	
Oxidant gas inlet temperature	5	TO1	Thermocouple type K	
Oxidant gas outlet temperature	8	TO2	Thermocouple type K	
Stack temperature	6	T0	Thermocouple type K	
Fuel gas inlet relative humidity	1	FR	PID temperature algorithm*	
Oxidant gas inlet relative humidity	3	OR	PID temperature algorithm	
Fuel inlet pressure	1	FPin	Pressure transducer	
Fuel outlet pressure	7	FPout	Pressure transducer	
Oxidant inlet pressure	3	OPin	Pressure transducer	
Oxidant outlet pressure	8	OPout	Pressure transducer	
Fuel pressure drop	@7 (7-1)	FPdrop	-	Calculated
Oxidant pressure drop	@8 (8-3)	OPdrop	-	Calculated
Fuel flow rate	1	FFlow	Mass flow controller	1/min
Oxidant flow rate	3	OFlow	Mass flow controller	
Purge flow rate	2	PFlow	Mass flow controller	

^- minimum sample rate available to GMS

Table 3: Variable measureable inputs.

Parameter name	**Range of operation**	**Unit**
Volumetric flow rate of Hydrogen	500-25000	Cm^3/min (standard cubic centimetres per minute) sccm
Volumetric flow rate of air	500-25000	sccm
Volumetric flow rate of Nitrogen	500-25000	sccm
Current load on fuel cell	0-1.5	A/cm^2

Table 4: Static measureable inputs.

Parameter name	**Range of operation**	**Unit**
Relative Humidity of Hydrogen	0.0/1.0	
Relative Humidity of air	0.0/1.0	
Pressure of Hydrogen	1.0-2.5	Bar
Pressure of air	1.0-2.5	Bar
Pressure of Nitrogen	1.0-2.5	Bar
Back pressure of Hydrogen	1.0-2.5	Bar
Back pressure of air	1.0-2.5	Bar
Back pressure of Nitrogen	1.0-2.5	Bar
Temperature of Hydrogen at given point	303-373	K
Temperature of air at given point *	303-373	K
Temperature of cell anode chamber	303-373	K
Temperature of cell cathode chamber	303-373	K

Table 5: Test measurable outputs

Parameter name	**Expected Range**	**Unit**
Voltage at anode	0.0-1.2	V
Voltage at cathode	0.0-1.2	V
Total voltage	0.0-1.2	V
Individual cell voltages	0.0-1.2	V
Average current density from cell	0.0-1.5	A/cm^2
Current produced from stack	0-100+	A
Power from stack	0-500	W
Water output	-	l/hour
Time	n/a	s
Resistance	-	Ohms
Temperature at cathode exit	303-373	K

Table 6: Measurable input uncertainty.

Input	**Value/ Range**	**Measurement uncertainty**	**Additional information**
Input Pressure (abs) (PH_2/Pair)	1.0-2.5 Bar	±1%	
Back pressure (BpH_2/Bpair)	1.0-2.5 Bar	±1%	
Composition fuel (φfuel)	~99.99%	±0.05%	
Composition oxidant (φox)	~21% O_2/79% N_2	±1% for O_2	
Composition purge (φpurge)	~99.99%	±0.05%	
Temp fuel_in	303-373 K	±2K	
Temp oxidant_in	303-373 K	±2K	
Temp stack	303-373 K	±2K	
Temp fuel_out	303-373 K	±2K	
Temp ambient	293K	±2K	
RH H2/air	~100 %	-5%	
Flow rate fuel (FFlow)	2500-25000 sccm	±1% F.S	Resolution: 0.1% F.S
Flow rate oxidant (OFlow)	2500-25000 sccm	±1% F.S	Resolution: 0.1% F.S
Flow rate purge (PFlow)	2500-25000 sccm	±1% F.S	Resolution: 0.1% F.S
Input electrical load	*See table 1	*see table 1	

Table 7: Measurable output uncertainty.

Type of output	**Measurement uncertainty**	**Additional information**
Stack voltage	See Table 1	
Cell voltage (voltage multiplexer)	±0.004% F.S Vdc 10V F.S	Based on a 1year reading @ 23°C ±5°C inclusive of measurement error, switching error and transducer conversion error.
Stack current	See Table 1	
Temp stack	±2K	
Temp fuel outlet	±2K	
Temp oxidant outlet	±2K	